Design of a Series of Preceramic *B*-Tri(methylamino)borazine-Based Polymers as Fiber Precursors: Architecture, Thermal Behavior, and Melt-Spinnability†

Sylvain Duperrier,‡ Christel Gervais,§ Samuel Bernard,*,‡ David Cornu,‡ Florence Babonneau,§ Corneliu Balan,⊥ and Philippe Miele*,‡

Laboratoire des Multimatériaux et Interfaces, UMR CNRS 5615, Université Claude Bernard Lyon 1, 43 Bd du 11 novembre 1918, Bâtiment Berthollet, 69622 Villeurbanne Cedex, France; Laboratoire de Chimie de la Matière Condensée, UMR CNRS 7574, Université Paris 6, 4 Place Jussieu, tour 54, étage 5, 75252 Paris Cedex, France; and REOROM Laboratory, Hydraulics Department, "Politehnica" University of Bucharest, Splaiul Independentei 313, 060032 Bucharest, Romania

Received October 5, 2006; Revised Manuscript Received November 30, 2006

ABSTRACT: A series of poly[*B*-(methylamino)borazine] were synthesized by thermolysis of a monomeric *B*-tri(methylamino)borazine at various temperatures between 150 and 200 °C and then characterized for suitability as a fiber precursor. Polymerization mechanisms and polymer architectures are discussed. It was shown that poly[*B*-(methylamino)borazine] represents a network combining a majority of $-N(CH_3)-$ bridges with a small proportion of B−N bonds, both connecting borazine rings, and $-N(H)CH_3$ groups. Both the ratio between flexible $-N(CH_3)-$ bridges and rigid B−N bonds and the relative amounts of plasticizing $-N(H)CH_3$ groups cause different responses to thermal properties and spinnability (glass transition, spinning temperatures, melt throughput, and fiber drawing). Based on fiber shape visualization using CCD camera during extrusion, appreciable melt-spinnable compounds are prepared between 160 and 185 °C. Such polymers display a chemical formula of $[B_{3.0}N_{4.4\pm0.1}C_{2.0\pm0.1}H_{9.3\pm0.2}]_n$ ($n \sim 7.5$), a glass transition between 64 and 83 °C, tailored flexibility, and sufficient plasticity to successfully produce fine-diameter green fibers.

1. Introduction

With the need for the development of non-oxide ceramics with high purity for thermostructural applications, the pyrolysis of inorganic precursors creates substantial interest, both scientifically and for practical purposes.[1−4] Such compounds provide a means for controlling and adjusting composition and nano/microstructure shaping of ceramic materials which allows the desired materials to be designed. This elegant chemical approach, the so-called polymer-derived ceramics (PDCs) route, has been introduced in the early 1960s by Poppers and Chantrell[4] and is mainly applied to the preparation of non-oxide ceramic fibers. Then, precursor-derived ceramic fibers were historically proposed by Yajima[5] and Verbeck[6] in the 1970s to Si/C/N(O) fibrous systems, and different compositions have been provided since then, most of them including Si-based ceramic fibers such as Si/C/N and Si/B/C/N systems.[7−9] In the case of fibers, the method consists of four major steps: (i) synthesis of a molecular precursor containing the constitutive elements of the desired ceramics in a homogeneous distribution, (ii) transformation of the precursor into a preceramic network with defined rheological behavior to provide proper processing capabilities, (iii) spinning of this preceramic polymer into a green fiber, and (iv) subsequent conversion of as-spun fibers to the desired ceramic fibers through appropriate thermal and/or chemical protocols under selected oxygen-free atmospheres. Twenty years ago, Wynne and Rice[10] rationalized this route, as they set a series of general empirical rules which are still valid for the design of suitable spinnable polymers.

Among non-oxide advanced ceramics, hexagonal boron nitride (*h*-BN) is an advanced ceramic that could offer great potentialities as fibrous reinforcing agent in specific applications.[11] *h*-BN[12−15] represents a crystalline ceramic with a layered anisotropic structure, similarly to that of carbon graphite. It offers some attractive properties such as high stiffness and toughness along the basal layers, a nonwettability against many metallic and silicate melts, a good oxidative resistance up to $T \sim 1000$ °C, and a low coefficient of thermal expansion in the direction of basal layers. In addition, this poorly dense ceramic ($d = 2.27$) exhibits potentialities in infrared and microwave-transparent structures and excellent electrical insulation properties. The main idea behind the preparation of BN fibers is to combine in a same fiber the high strength of polyacrylonitrile-derived carbon fibers with the specific properties of *h*-BN.

Although controlling the various demands with respect to processing of ceramic fibers, i.e., fusibility and/or solubility, thermal stability at low temperature for melt-spinning, and high ceramic yield, and combining them in only one molecule remains an ambitious objective, preceramic polymers which use the borazine ring as a basal structural unit can be well suited for filling the requirements as BN fiber precursor.[11−22] As an illustration, several attempts were successful in our lab for producing BN fibers with high mechanical performances from *B*-tri(methylamino)borazine-based polymers, namely poly[*B*-(methylamino)borazine].[20]

However, the preparation of poly[*B*-(methylamino)borazine]-derived BN fibers remains a complex and difficult task in terms of polymer synthesis and spinning, resulting in a lack of reproducibility in mechanical performance. Such variations in

* Corresponding authors. E-mail: Samuel.Bernard@univ-lyon1.fr, Philippe.Miele@univ-lyon1.fr; Tel: +33 472 433 612; Fax: +33 472 440 618.

† We wish to dedicate this paper to the memory of Dr. Jean-Marie Létoffé, who managed the center of thermal analyses in the Laboratoire des Multimatériaux et Interfaces.

‡ Université Claude Bernard Lyon 1.

§ Université Paris 6.

⊥ "Politehnica" University of Bucharest.

10.1021/ma0623035 CCC: $37.00
Published on Web 01/18/2007

the quality of the final fibers are the result of the nature and structure of these polymers and the thermal and rheological phenomena that occur during their spinning. It is therefore our intent to investigate the synthesis and spinning of a set of representative poly[*B*-(methylamino)borazine] and understand the role of their architecture on their thermal and rheological behavior upon melt-spinning through two papers . The first aim of the present paper is to ascertain the chemical steps and establish the structural changes which occur during the polymer preparation using a combination of ^{15}N solid-state NMR, GC/MS, elemental analyses, and density measurements. Second, we investigate the thermal properties and the spinning behavior of polymers using thermal analysis and CCD camera visualization of fiber geometry during extrusion and fiber drawing. We therefore discuss the effects of architecture on the thermal behavior and spinnability of poly[*B*-(methylamino)borazine], and we provide synthesis conditions that allow us to develop melt-spinnable polymers. In the following paper, we will describe how polymer architecture affects shear rheology behavior of polymer melts and provides reliable melt-spinnability assumptions that help us to predict the melt-spinnability of poly[*B*-(methylamino)borazine]. It should be mentioned that the literature dedicated to melt-spinning of preceramic polymers is rather scarce,[7−9,23−27] and to our knowledge, there are no detailed reports focused on the effects of polymer architecture on thermal, spinning, and rheological behavior of preceramic polymers as fiber precursors.

2. Experimental Section

2.1. General Comment. Syntheses were carried out in an argon atmosphere, using argon/vacuum lines and Schlenk-type flasks. Argon (>99.995%) was purified by passing through successive columns of phosphorus pentoxide, siccapent, and BTS catalysts. Purified *B*-tri(chloro)borazine was purchased from Katchem Ltd. (Praha, Czech Republic). This molecule was analyzed by ^1H and ^{11}B NMR and IR spectroscopies. ^{11}B NMR (96.29 MHz, C_6D_6, ppm): 29.7 (br). ^1H NMR (300 MHz, $CDCl_3$, ppm): 5.29 br (N(*H*) borazine). IR data (KBr pellets, cm^{-1}): 3450 (m); 1438 (s); 1031 (m), 743 (w), 704 (w).

Methylamine (99+%) obtained from Sigma Aldrich was purified by passing through a column of potassium hydroxide. Toluene was dried and purified using standard glass manipulation and was freshly distilled under argon from sodium/benzophenone prior to use. Preparation of samples for characterization was performed inside an argon-filled glovebox (Jacomex BS521; Dagneux, France).

2.2. Synthesis of Molecular and Polymer Precursors. *B*-tri(methylamino)borazine was prepared in a three-necked 2 L Schlenk flask equipped with a methanol reflux condenser by dropping a solution of 77 g of *B*-tri(chloro)borazine (419 mmol) in toluene on a solution of 105 g (3.387 mol) of methylamine in toluene, at −50 °C with vigorous magnetic stirring, whereby methylamine hydrochloride precipitation was observed immediately. After the addition of *B*-tri(chloro)borazine was complete, the reaction mixture was allowed to warm to room temperature (RT). The precursor solution was then separated from the precipitated methylamine hydrochloride by filtration through a pad of Celite. The precipitate was thoroughly extracted three times with 50 mL of toluene and then disposed. The filtrate and the extract were combined, and toluene was partially removed at RT in high vacuum (10^{-1} mbar) from the remaining solution until the concentration of the *B*-tri(methylamino)borazine (**1**) in toluene reached 65 wt %. It should be mentioned that the *B*-tri(methylamino)borazine was partially dried to facilitate its introduction in the polymerization reactor for the subsequent thermolysis step.

Synthesis of the poly[*B*-(methylamino)borazines] **2**−**6** proceeded as follows.

A 250 mL three-necked polymerization reactor equipped with a mechanical stirrer was charged at RT with 70 g (419 mmol) of the solution of **1**. The mixture was heated in vacuum to 75 °C with vigorous stirring to remove residual toluene, giving 45.5 g (267.2 mmol) of product. The reaction was continued in a flowing argon (3 L/h) at $P_{Ar} = 1$ atm step by step to the desired final synthesis temperature ($T_{thermolysis}$) ranging from 150 °C (polymer **2**) to 200 °C (polymer **6**). After cooling to RT, poly[*B*-(methylamino)-borazines] **2**−**6** were recovered as air- and moisture-sensitive solids. Samples were stored inside an argon-filled glovebox.

Polymer **2**: $T_{thermolysis} = 150$ °C. IR data (KBr pellets, cm^{-1}): 3434 (m); 2958 (w) 2928 (w), 2898 (w), 2820 (m); 1597 (s); 1515 (s); 1460 (s); 1411 (s); 1178 (s); 1095 (m), 707 (w). ^{11}B NMR (96.29 MHz, C_6D_6, ppm): 25.7 (br). ^1H NMR (300 MHz, CD_2Cl_2, ppm): 1.86 br (−N(*H*)CH_3); 2.47 vbr (−N(H)C*H*$_3$); 2.56 vbr (bridging −N(C*H*$_3$)−); 2.70−4.10 br (N(*H*) borazine). ^{13}C NMR (75 MHz, CD_2Cl_2, ppm): 27.6, 27.9 (−N(H)*C*H_3); 31.2 (bridging −N(*C*H_3)−). TGA (ammonia, 1000 °C (1 °C/min); 47.3% weight loss): 0−45 °C, $\Delta m/m_0 = 0\%$; 45−400 °C, $\Delta m/m_0 = 26.8\%$; 400−1000 °C, $\Delta m/m_0 = 20.5\%$.

Polymer **3**: $T_{thermolysis} = 160$ °C. IR data (KBr pellets, cm^{-1}): 3430 (m); 2936 (w), 2894 (w), 2816 (m); 1597 (s); 1519 (s); 1460 (s); 1413 (s); 1182 (s); 1091 (m), 707 (w). ^{11}B NMR (96.29 MHz, C_6D_6, ppm): 25.77 (br). ^1H NMR (300 MHz, CD_2Cl_2, ppm): 1.86 br (−N(*H*)CH_3); 2.47 vbr (−N(H)C*H*$_3$); 2.55 vbr (−N(C*H*$_3$)−); 2.64−3.37 br (N(*H*) borazine). ^{13}C NMR (75 MHz, CD_2Cl_2, ppm): 27.6, 27.9 (−N(H)*C*H_3); 31.2 (bridging −N(*C*H_3)−). TGA (ammonia, 1000 °C (1 °C/min); 46.3% weight loss): 0−45 °C, $\Delta m/m_0 = 0\%$; 45−400 °C, $\Delta m/m_0 = 25.4\%$; 400−1000 °C, $\Delta m/m_0 = 20.9\%$.

Polymer **4**: $T_{thermolysis} = 175$ °C. IR data (KBr pellets, cm^{-1}): 3434 (m); 2958 (w) 2928 (w), 2898 (w), 2820 (m); 1597 (s); 1515 (s); 1460 (s); 1411 (s); 182 (s); 1088 (m), 707 (w). ^{11}B NMR (96.29 MHz, C_6D_6, ppm): 25.77 (br). ^1H NMR (300 MHz, CD_2Cl_2, ppm): 1.86 br (−N(*H*)CH_3); 2.47 vbr (−N(H)C*H*$_3$); 2.55 vbr (−N(C*H*$_3$)−); 2.64−3.37 br (N(*H*) borazine). ^{13}C NMR (75 MHz, CD_2Cl_2, ppm) 27.6, 27.9 (−N(H)*C*H_3); 31.2 (bridging −N(*C*H_3)−). TGA (ammonia, 1000 °C (1 °C/min); 45.5% weight loss): 0−45 °C, $\Delta m/m_0 = 0\%$; 45−400 °C, $\Delta m/m_0 = 24.0\%$; 400−1000 °C, $\Delta m/m_0 = 21.5\%$.

Polymer **5**: $T_{thermolysis} = 185$ °C. IR data (KBr pellets, cm^{-1}): 3435 (m); 2958 (w), 2893 (w), 2817 (m); 1597 (s); 1515 (s); 1460 (s); 1418 (s); 1187 (s); 1087 (m), 710 (w). ^{11}B NMR (96.29 MHz, C_6D_6, ppm): 25.77 (br). ^1H NMR (300 MHz, CD_2Cl_2, ppm): 1.86 br (−N(*H*)CH_3); 2.47 vbr (−N(H)C*H*$_3$); 2.55 vbr (−N(C*H*$_3$)−); 2.64−3.37 br (N(*H*) borazine). ^{13}C NMR (75 MHz, CD_2Cl_2, ppm): 27.6, 27.9 (−N(H)*C*H_3); 31.2 (bridging −N(*C*H_3)−). TGA (ammonia, 1000 °C (1 °C/min); 42.5% weight loss): 0−45 °C, $\Delta m/m_0 = 0\%$; 45−400 °C, $\Delta m/m_0 = 21.6\%$; 400−1000 °C, $\Delta m/m_0 = 20.9\%$.

Polymer **6**: $T_{thermolysis} = 200$ °C. IR data (KBr pellets, cm^{-1}): 3434 (m); 2936 (w), 2893 (w), 2816 (m); 1601 (s); 1528 (s); 1460 (s); 1433 (s); 1187 (s); 1087 (m), 711 (w). ^{11}B NMR (96.29 MHz, C_6D_6, ppm): 25.77 (br). ^1H NMR (300 MHz, CD_2Cl_2, ppm): 1.86 br (−N(*H*)CH_3); 2.47 vbr (−N(H)C*H*$_3$); 2.55 vbr (−N(C*H*$_3$)−); 2.64−3.37 br (N(*H*) borazine). ^{13}C NMR (75 MHz, CD_2Cl_2, ppm): 27.6, 27.9 (−N(H)*C*H_3); 31.2 (bridging −N(*C*H_3)−). TGA (ammonia, 1000 °C (1 °C/min); 41.6% weight loss): 0−45 °C, $\Delta m/m_0 = 0\%$; 45−400 °C, $\Delta m/m_0 = 19.2\%$; 400−1000 °C, $\Delta m/m_0 = 22.4\%$.

2.3. Melt-Spinning. Polymers **2**−**6** were tested with regard to melt-spinning combining a lab-scale piston extrusion system (Matériau Ingéniérie-St-Christol les Alès, France) to melt the polymer and to supply definite throughputs and a wind-up device, i.e., spool, to supply the take-up velocity, both set up in a nitrogen-filled glovebox (Figure 1).

The distance from the rotating spool to the spinneret was fixed at 18 cm. Extrusion and drawing units are designed for small-scale spinning and can support flow throughputs from 0.1 to 2 mm/min and take-up velocity from 9 to 330 m/min. The piston chamber can support an internal pressure of 600 N. Four grams of solid polymers was placed at RT into the piston chamber and heated (5 °C/min) without compressive load to a certain temperature, namely

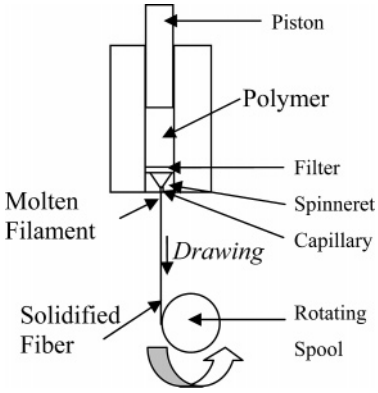

Figure 1. Description of the melt-spinning process.

$T_{spinning}$. At $T_{spinning}$, the polymer melt flow was forced by pushing it with the piston along the extrusion line through a melt filtering and then a single-capillary spinneret of 200 μm in diameter akin to liquid being squirted out of the capillary at a controlled piston velocity. As-extruded molten filament fell with gravity at an ideal pressure of ~350 N to be drawn during cooling by the take-up spool and continuously recovered onto the spool. It should be mentioned that the process of producing BN fibers continues through a curing step of green fibers in an ammonia atmosphere (RT to 400 °C) to retain fiber integrity, i.e., avoid melting of the polymer fibers, during the further pyrolysis. The latter is performed in an ammonia atmosphere (400−1000 °C) to remove carbon residues and then in a nitrogen atmosphere (1000−1800 °C) to achieve the complete ceramic transformation.[28]

2.4. Polymer and Green Fiber Characterization. *2.4.1. ^{15}N Solid-State NMR.* ^{15}N solid-state NMR experiments were performed at RT on a Bruker Avance-300 spectrometer, at a frequency of 30.41 MHz using a Bruker magic angle spinning (MAS) probe. Solid samples were spun at 5 kHz, using 7 mm ZrO_2 rotors filled up inside an argon gas glovebox. ^{15}N MAS NMR spectra were recorded with a pulse angle of 90° and a recycle delay between pulses of 100 s. ^{15}N chemical shifts were referenced to solid NH_4NO_3 (10% ^{15}N-enriched sample, $\delta_{iso}(^{15}NO_3) = -4.6$ ppm compared to CH_3NO_2 ($\delta_{iso}(^{15}NO_2) = 0$ ppm)), and spectra were simulated with DMFIT.[29−31] ^{15}N-enriched polymers **2**−**6** were obtained from a same batch of ^{15}N-enriched **1**. The latter was synthesized by aminolysis of a ^{15}N-enriched *B*-tri(chloro)borazine using homemade methylamine ^{15}N enriched at 10 at. %.[28]

2.4.2. Elemental Analyses. Elemental analyses were made at the Max-Planck Institute (Stuttgart, Germany) using various apparatus (ELEMENTAR, Vario EL CHN-Determinator; ELTRA, CS 800, C/S Determinator; LECO, TC-436, N/O Determinator, and atom emission spectrometry (ISA JOBIN YVON JY70 Plus).

2.4.3. GC/MS. GC/MS measurements were performed in a continuous thermolysis process using a Hewlett-Packard model Agilent micro-GC M200 equipment coupled with a quadripole mass spectrometer (Agilent 5973 network mass selective detection). Gaseous species were identified on the basis of their MS molecular ion peaks and by comparison of the GC retention times of their corresponding GC signals to those of known gas such as hydrogen, ammonia, methylamine, or argon. A quantitative GC analysis was carried out from the area of the signals. Signal areas were normalized to the same, overall, integrated area values.

2.4.4. Differential Scanning Calorimetry (DSC). DSC measurements were carried out on a TA8000 Mettler-Toledo apparatus, using alumina crucibles in a nitrogen atmosphere and the following temperature program: −30 to 200 °C (10 °C/min).

2.4.5. Picnometry. Density measurements were carried out at RT in a controlled inert environment with a density analyzer (AccuPyc 1330 Helium pycnometer from Micromeritics).

2.4.6. Size Exclusion Chromatography (SEC). Molecular weight distribution was determined by SEC. Analysis was performed using a Shimadzu SPD 6A UV detector and Waters s-Styragel columns in distilled tetrahydrofuran (THF; Sigma-Aldrich) as eluent with *N*,*N*-dimethylacetamide (DMAC). A calibration curve was generated from the chromatograms of the *B*-tri(methylamino)borazine (M = 167.6 g/mol).

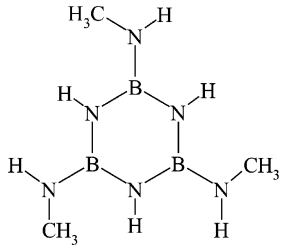

Figure 2. Schematic representation of the *B*-tri(methylamino)borazine.

2.4.7. Fiber Shape Visualization. Green fiber pictures were recorded during melt-spinning operation using a Sony DXC-9100P 3CCD camera equipped with a 40× zoom. The camera resolution was 782 × 582 pixels (800 vertical lines × 575 horizontal lines). Pictures were analyzed using the Analysis software, and precision of the diameter measurements was of 1 pixel (<2% of diameter).

2.4.8. Polarized Light. A Nikon Optiphot-pol polarized light microscope equipped with crossed polarizers and a rotating stage was used to investigate the effect of fiber drawing during melt-spinning on the molecular orientation in as-spun fibers. Orientation was revealed by transmitted light for an angle of 45° between the fiber and the polarizer direction.

3. Results and Discussion

3.1. Design of Poly[*B*-(methylamino)borazine] with Defined Architecture. In the present work, the same batch of *B*-tri(methylamino)borazine (**1**) (Figure 2) was thermolyzed in argon between 150 and 200 °C forming solid polymeric networks, namely poly[*B*-(methylamino)borazine], with defined architectures, thermal properties, and melt-spinnabilities. The synthetic procedure must be carefully controlled since successful spinning is directly connected to the structural properties of the polymer, which are closely dependent on the synthesis conditions. To establish synthesis conditions that allow preparation of melt-spinnable polymers, the architecture and chemistry of a set of five representative preceramic polymers **2** ($T_{thermolysis}$ = 150 °C) to **6** ($T_{thermolysis}$ = 200 °C) were characterized at RT.

It should be mentioned that the term "polymer" is used in its broadest sense, that is, as a group of molecules whose structure can be generated through repetition of a few elementary borazine units.

In a previous study,[28] it was shown that a poly[*B*-(methylamino)borazine] ($[B_{3.0}N_{4.6}C_{2.1}H_{9.5}]_n$) obtained at $T_{thermolysis}$ = 180 °C comprises at least four types of nitrogen environments using CP and IRCP sequences to distinguish the degree of protonation (see Figure 1-SI in Supporting Information).

It was found that the overall structure of the studied poly[*B*-(methylamino)borazine] built from borazine rings contains the expected borazine *N*H units (δ_{iso} = −307 ppm) and is dominated by bridging $-N(CH_3)-$ units (δ_{iso} = −320 ppm) connecting the rings to the others. In addition, some $-N(H)-CH_3$ groups (δ_{iso} = −347 ppm) present in the starting monomer **1**[32] survive in the derived polymer backbone (see Figure 2-SI in Supporting Information). Interestingly, a low relative amount of unexpected NB_3 sites (δ_{iso} = −285 ppm) is also identified, but some doubts arise for the correct attribution of the corresponding structural motif. Three types of motifs were proposed (see Figure 3-SI in Supporting Information).[28]

In order to get a better understanding of the architecture of the poly[*B*-(methylamino)borazine] and to provide a complete diagnostic of its properties, our efforts focus on the synthesis of several poly[*B*-(methylamino)borazine] and the use of

Scheme 1. Condensation Reaction of $-N(H)CH_3$ Groups Resulting in Both the Formation of Bridged $-N(CH_3)-$ Units and the Release of Methylamine

combined characterization techniques including gas chromatography coupled with mass spectrometry (GC/MS), ^{15}N solid-state NMR, chemical analyses, and picnometry. The chemical reactions occurring during thermolysis of **1** were monitored by GC/MS, which allows us to offer a schematic representation of chemical reactions that emerge during this process. The related architectural changes taking place during thermolysis were analyzed on the basis of representative polymer samples described in the Experimental Section using ^{15}N solid-state NMR, and elemental analyses. Density measurements of these polymers by picnometry were also obtained.

According to GC/MS experiments, the transformation of **1** into the derived polymers **2**−**6** occurs mainly with loss of methylamine (CH_3NH_2; $m/z = 31$) (see Figure 4-SI in Supporting Information). This should form $-N(CH_3)-$ bridging borazine rings ($\delta_{iso} = -320$ ppm), as depicted in Scheme 1.

Quantitative analysis of ^{15}N solid-state NMR data of polymers **2**−**6** presented in Figure 3 and Table 1 confirms this suggestion. Figure 3 includes the experimental and simulated ^{15}N MAS NMR spectra of **2**, **4**, and **6**, and Table 1 gives the ^{15}N chemical shifts and relative amounts of the structural units extracted from the NMR spectra of each polymer.

^{15}N MAS NMR data point to an increase in the relative amounts of $-N(CH_3)-$ bridges ($\delta_{iso} = -320$ ppm) going from **2** to **6**, whereas the relative amounts of $-N(H)CH_3$ ($\delta_{iso} = -347$ ppm) decrease. This agrees with the polycondensation mechanism proposed in Scheme 1. It is even shown that this mechanism is mainly effective at low temperature ($T_{thermolysis} \leq 160$ °C) by plotting the ratio of $-N(CH_3)-$ bridges to $-N(H)CH_3$ groups in Figure 4 (empty square symbols).

It should be mentioned that this experimental curve is plotted using a sigmoidal-type function and also by considering additional polymeric intermediates prepared at 130, 140 (not published polymers), and 180 °C[28] following the procedure described in the Experimental Section.

The occurrence of the above-described polycondensation mechanism is consistent with the studies dedicated to the synthesis of borazine-type polymers[33,34] in which the thermolysis of monomeric borazine derivatives is shown to predominantly proceed via intermolecular condensation of $-N(H)R$ groups (R = H, CH_3).

It is interesting to note in Table 1 a decrease in the relative amounts of borazine N(*H*) units ($\delta_{iso}(^{15}N) = -307$ ppm) starting from **4**, whereas they should either be stable (formation of a linear structure) or increased (formation of a branched structure) during thermolysis of **1** by considering the occurrence of the mechanism depicted in Scheme 1. This highlights the presence of a concurrent mechanism including participation of borazine NH units.

A second route generating alkylamine species through polycondensation reactions including borazine N(H) units has been reported for *B*-tri(amino/alkylamino)borazines.[35] It consists in the formation of boron−nitrogen (B−N) bonds connecting two borazine rings yielding the NB_3-containing motif **II** we have already proposed in ref 28. In our system, this mechanism occurs from the reaction of borazine N(H) units with $-N(H)CH_3$ groups generating methylamine (Scheme 2).

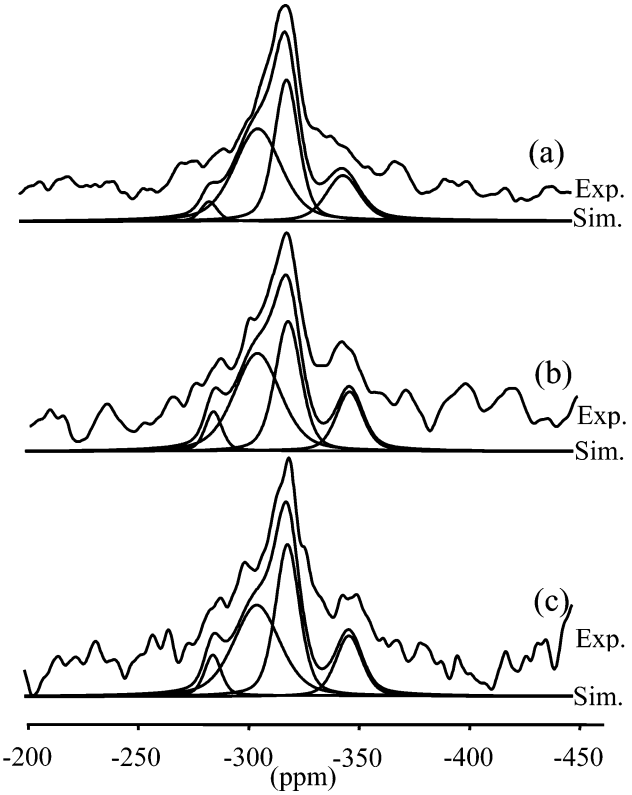

Figure 3. Selected experimental and simulated ^{15}N solid-state MAS NMR of the ^{15}N-enriched poly[*B*-(methylamino)borazine]: (a) **2** ($T_{thermolysis} = 150$ °C), (b) **4** ($T_{thermolysis} = 175$ °C), and (c) **6** ($T_{thermolysis} = 200$ °C).

The increase in the relative amounts of NB_3 sites associated with the disappearance of borazine N(H) units from **2** to **6** (Table 1) is entirely consistent with the mechanism depicted in Scheme 2. By plotting the $-NB_3$ to N(H) ratio in Figure 4 (black circles) using a sigmoidal-type function, this second mechanism is seen to mainly occur after the first one; i.e., it is mainly effective above 160 °C. This is most probably attributed to the greater thermal stability of N−H bonds of borazine rings compared to the N−H bonds in $-N(H)CH_3$ groups.

To our knowledge, any other reactions generating methylamine can be considered taking into account the functional groups, i.e., borazine N(H) units and $-N(H)CH_3$ groups, which are present in the monomeric *B*-tri(methylamino)borazine (compound **1**).

Whereas the production of methylamine during thermolysis of *B*-tri(methylamino)borazine was foreseeable according to the presence of $-N(H)CH_3$ groups in **1**, the identification of ammonia (NH_3; $m/z = 17$) as a second gaseous byproduct by GC/MS was not expected (see Figure 4-SI in Supporting Information). Further, the CH_3NH_2:NH_3 ratio decreases from 5000 at 120 °C to 9.5 at 200 °C based on the relative area of the corresponding GC signals. Therefore, production of ammonia increases with increasing $T_{thermolysis}$.

Evolution of ammonia suggests the presence of $-NH_2$ groups in the polymeric network. Considering that such highly reactive groups are not identified by NMR and IR spectroscopies (see experimental part and Table 1), it can be assumed that either their relative amount is too low or they quickly react to form more thermally stable species.

On the basis of the actual knowledge of the chemistry of borazine-derived molecules, the only mechanism explaining the appearance of $-NH_2$ groups is a highly energetic ring-opening pathway. Such mechanisms historically proposed by Toenisko-

Table 1. Variation of Relative Amounts of −N(CH$_3$)− Bridges, −N(H)CH$_3$ Groups, Borazine N(H) Units, and NB$_3$ Sites in Polymers Based on the Relative Intensity of the Related ^{15}N MAS NMR Signals for Each ^{15}N-Enriched Poly[*B*-(methylamino)borazine] 2−6

		relative intensity [%] (±2)			
polymer	$T_{thermolysis}$ [°C]	$\%_{-N(H)CH_3\ groups}$ $\delta_{iso} = -347$ ppm	$\%_{-N(CH_3)-\ bridges}$ $\delta_{iso} = -320$ ppm	$\%_{N(H)\ units}$ $\delta_{iso} = -307$ ppm	$\%_{NB_3\ sites}$ $\delta_{iso} = -285$ ppm
2	150	16	35.7	44.9	3.4
3	160	15	35.7	44.8	4.5
4	175	14.2	35.9	44.9	6.5
5	185	13.8	36.2	43.2	6.8
6	200	13.6	37	42.6	6.8

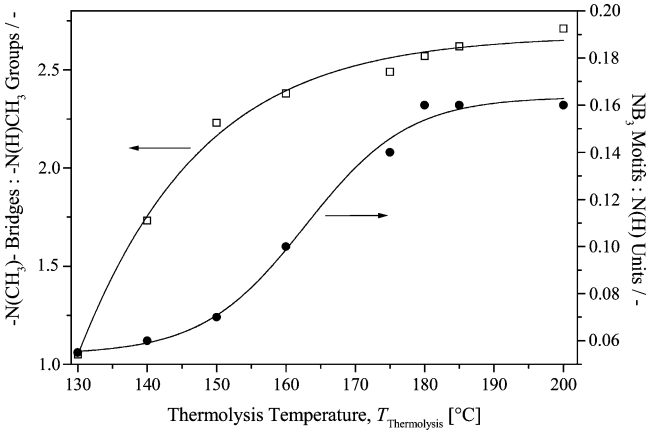

Figure 4. Variation of the −N(CH$_3$)− bridges:−N(H)CH$_3$ groups ratio (empty square symbols) and NB$_3$ motifs:borazine N(H) units ratio (black circle symbols) during thermolysis of **1**.

Scheme 2. Condensation Reaction of −N(H)CH$_3$ Groups with Borazine N(H) Resulting in Both the Formation of B−N Bonds and the Release of Methylamine

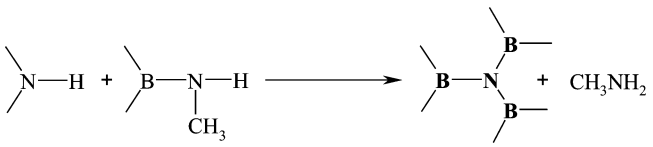

Scheme 3. Ring-Opening Mechanism Leading to Formation of −NH$_2$ Groups

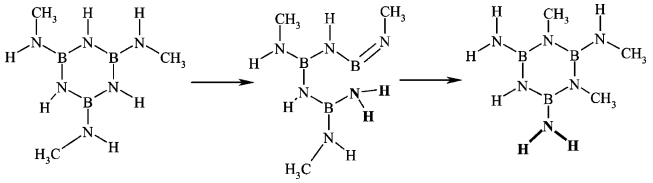

etter et al. have been postulated to be activated when the borazine derivative contains −N(H)R (R = H, CH$_3$) units bonded to boron atoms.[37,38] Scheme 3 illustrates the most probable ring-opening mechanism occurring in our system, which implies also the formation of a new B$_2$N(CH$_3$) unit in the as-obtained structure.

According to their relatively high thermal reactivity, these −NH$_2$ groups should react with borazine N(H) units and/or −N(H)CH$_3$ groups with subsequent expulsion of ammonia and/or methylamine. Bridging −N(H)− units and inter-ring B−N bonds, i.e., NB$_3$ motifs, should then result (see Scheme 1-SI in Supporting Information). According to the increase in ammonia production with increasing $T_{thermolysis}$, the proportion of structural units formed must increase on going from **2** to **6**.

The structural changes previously evidenced do not have a strong impact on the polymer chemistry, as illustrated with elemental analyses.

Polymers **2**−**6** display close empirical formulas (Table 2; oxygen values were determined to be <2 wt % and were therefore omitted), indicating in a first approximation that the overall structure of the poly[*B*-(methylamino)borazine] established after synthesis at 150 °C is not significantly changed above that temperature.

Table 2. Elemental Composition and Formulas of Samples 1−6

	found composition[a] [wt %]				
samples	B	N	H	C	empirical formula[b]
monomer					
1[c]	19.4	50.1	9.0	21.5	$B_{3.0}N_{6.0}C_{3.0}H_{15.0}$
polymers					
2	24.1	46.9	7.6	21.4	$B_{3.0}N_{4.5}C_{2.4}H_{10.1}$
3	24.9	48.4	7.4	19.3	$B_{3.0}N_{4.5}C_{2.1}H_{9.6}$
4	25.5	48.5	7.4	18.6	$B_{3.0}N_{4.4}C_{2.0}H_{9.3}$
5	25.7	48.4	7.3	18.6	$B_{3.0}N_{4.3}C_{1.9}H_{9.1}$
6	26.5	48.1	7.2	18.2	$B_{3.0}N_{4.2}C_{1.9}H_{8.7}$

[a] Referenced to 100%; oxygen values were determined to be <2 wt % and were omitted. [b] Empirical formula per monomer unit and normalized to three B atoms. [c] Assuming the idealized structure presented in Figure 1.

The nitrogen composition for **2** ($[B_{3.0}N_{4.5}C_{2.4}H_{10.1}]_n$) and **3** ($[B_{3.0}N_{4.5}C_{2.1}H_{9.6}]_n$) agrees reasonably well with the theoretical value for a polymer composed exclusively of −N(CH$_3$)− bridges ($[B_{3.0}N_{4.5}C_{1.5}H_{7.5}]_n$). In contrast, the nitrogen composition from **4** ($[B_{3.0}N_{4.4}C_{2.0}H_{9.3}]_n$) to **6** ($[B_{3.0}N_{4.2}C_{1.9}H_{8.7}]_n$) clearly points to formation of cross-links connecting the borazine rings at several points of the same polymer chain in the high-temperature regime of the thermolysis.

The relatively high deviation between the compositions in carbon and hydrogen found in **2**−**3** and theory (exclusive formation of −N(CH$_3$)− bridges; see theoretical formula above) suggests the presence of unreacted −N(H)CH$_3$ groups. It is interesting to notice that the found values for carbon and hydrogen elements in such polymers are close to those expected for a poly[*B*-(methylamino)borazine] composed of −N(CH$_3$)− units connecting two borazine rings and one −N(H)CH$_3$ groups per borazine ring ($[B_{3.0}N_{5.0}C_{2.0}H_{10.0}]_n$, see Scheme 2-SI in Supporting Information). This confirms (i) the establishment of −N(CH$_3$)− bridges and (ii) the presence of a relatively high proportion of −N(H)CH$_3$ groups in the polymer network prepared in the low-temperature regime of the thermolysis. The loss of carbon and nitrogen elements from **3** to **6** indicates the gradual disappearance of −N(H)CH$_3$ groups with increasing $T_{thermolysis}$ and therefore the tendency of the polymers **4**−**6** to cross-link upon heating via the polycondensation mechanisms mentioned above. Such a behavior is confirmed by picnometry.

Density measurements of polymers were run at RT to follow the development of the polymer architecture during thermolysis. Some additional polymeric samples prepared at 130, 140 (not published polymers), and 180 °C[28] following the procedure described in the Experimental Section were analyzed to have a good representation of the density variation. Variation of poly[*B*-(methylamino)borazine] density is plotted in Figure 5. A sigmoidal-type function was used to fit the experimental data representing the variation of the density measured at RT as a function of the temperature at which polymers were prepared.

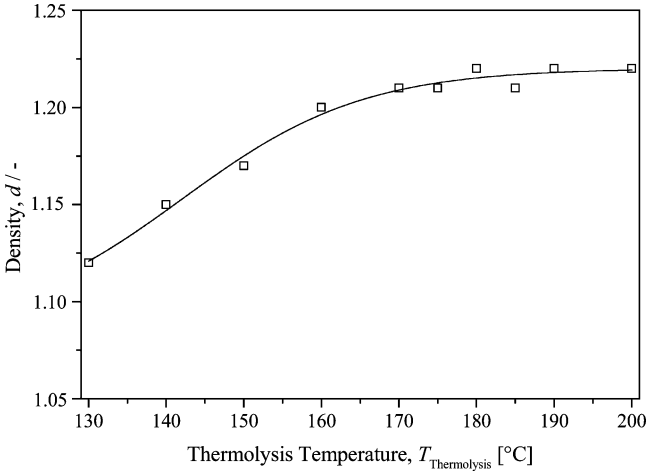

Figure 5. Density measurements of polymers obtained by thermolysis of **1** at various $T_{thermolysis}$.

Based on the density increase below 160 °C, an extension of the molecular network of **1** dominates upon heating in the low-temperature regime of the thermolysis. This behavior can be understood by considering the structure of the *B*-tri(methylamino)borazine composed of three $-N(H)CH_3$ groups and three borazine N(H) units (Figure 2), every one being subject to facile condensation reactions. Despite difference in chemical reactivity between $-N(H)CH_3$ groups and borazine N(H) units, it is reasonable to propose that *B*-tri(methylamino)borazine has a maximal functionality of six, which offers high potentialities to extend upon heating. Density values are not significantly changed above 160 °C. We may therefore suggest that intramolecular cross-linking plays a major role in the architecture development during thermolysis in the high-temperature regime.

As a consequence of the characterization results, it can be proposed that the basal structure of poly[*B*-(methylamino)-borazine] composed of a majority of inter-ring $-N(CH_3)-$ bridges is shaped at $T_{thermolysis} = 150$ °C. A relatively high amount of unreacted $-N(H)CH_3$ groups remains, suggesting a poorly cross-linked network. Above that thermolysis temperature, inter-ring B−N bonds, i.e., NB_3 sites, are gradually formed in such a way that the B/N ratio increases in the derived polymer network synthesized up to 200 °C. In addition, the decrease in the relative amounts of $-N(H)CH_3$ groups associated with the poor changes in the polymer density in the temperature range 160−200 °C indicates that the poly[*B*-(methylamino)borazine] cross-links on itself in the high-temperature regime of the thermolysis. Last, in relation with the detection of ammonia, it should be mentioned that −N(H)− bridges/NH_2 groups are formed, but despite a probable increase of their proportion going from **2** to **6**, their influence on the architecture of poly[*B*-(methylamino)borazine] remains poor.

3.2. Thermal Behavior of As-Synthesized Polymer. Solid poly[*B*-(methylamino)borazine] probably represents one of the few borazine-derived preceramic polymers capable of displaying glass transition temperatures T_g upon heating (Table 3).[11−22,28]

It should be mentioned that its glass transition extends over a wide temperature range (∼20 °C) which may be interpreted as a high molar mass dispersion in polymers. T_g values were taken at the middle of this temperature range on the differential scanning calorimetry (DSC) curve.

Solid poly[*B*-(methylamino)borazine] transforms into viscous materials by passing through T_g which rise from 46 (**2**) to 100 °C (**6**), as reported in Table 3.

To obtain an accurate representation of the change of T_g during polymer preparation, the variation of T_g as a function of

Table 3. Glass Transition Temperatures (T_g) and Limit Temperatures (T_ls) for Each Poly[*B*-(methylamino)borazine] 2−6

polymer	$T_{thermolysis}$ [°C]	T_g [°C]	T_l[a] [°C]
2	150	46	150
3	160	64	160
4	175	70	175
5	185	83	185
6	200	100	200

[a] T_l is the temperature at which a strong exothermic peak due to the polymer decomposition is observed in DSC curves.

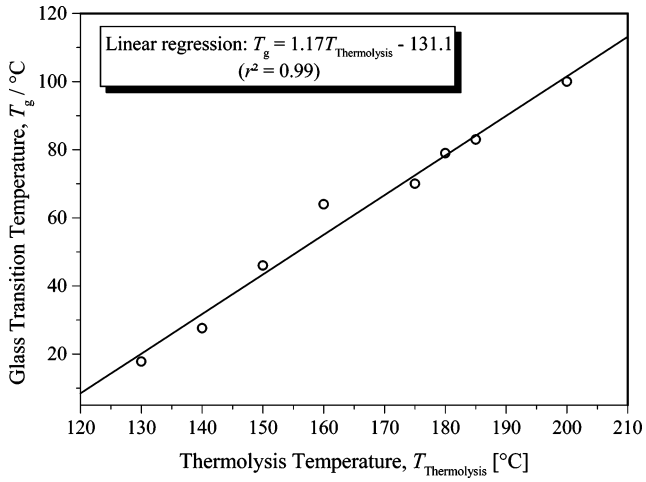

Figure 6. Variation of T_g as a function of $T_{thermolysis}$.

$T_{thermolysis}$ was studied using the five polymers described in experimental part and those we have already considered for plotting the density curve (Figure 5). Figure 6 shows that the values of T_g can be tuned by selecting $T_{thermolysis}$, since they linearly increase with increasing $T_{thermolysis}$ according to eq 1.

$$T_g = 1.17T_{thermolysis} - 131.1 \quad (1)$$

T_g values reach a plateau at 108 °C, since polymer samples prepared above 200 °C have no T_g.

In a first approximation, the evolution profile of T_g for poly-[*B*-(methylamino)borazine] seems to be similar to that observed for traditional organic polymers which obey the Flory−Fox law; i.e., T_g increase with increasing average values of the molecular weight (M_w) up to a certain value at which any changes in T_g are detected.[39,40]

We have therefore attempted to measure the molecular weight of every one of the poly[*B*-(methylamino)borazine] described in the experimental part. However, it should be mentioned that attempts to have a precise idea of the chain length failed, since the found values for the five polymers are too close to distinguish each poly[*B*-(methylamino)borazine] by their proper M_w ($M_w = 900 \pm 100$ g/mol for **2**−**5** and 1250 g/mol for **6**), despite strong differences in T_g. Therefore, such oligomeric compounds do not obey the Flory−Fox law. It is more appropriate to suggest that the strong increase of T_g from **2** to **6** is caused by the capability of poly[*B*-(methylamino)borazine] to undergo intramolecular cross-linking upon heating and is related to the nature and relative amount of structural units which compose the polymer network. Our suggestions are developed below.

First, pendent $-N(H)CH_3$ groups attached to boron atoms fulfill the requirements of limiting the chain branching, and therefore lowering the temperature of the solid-to-glass rubber transition, in the same way as a plasticizer acts to make a polymer more pliable and easier to work upon heating. Second,

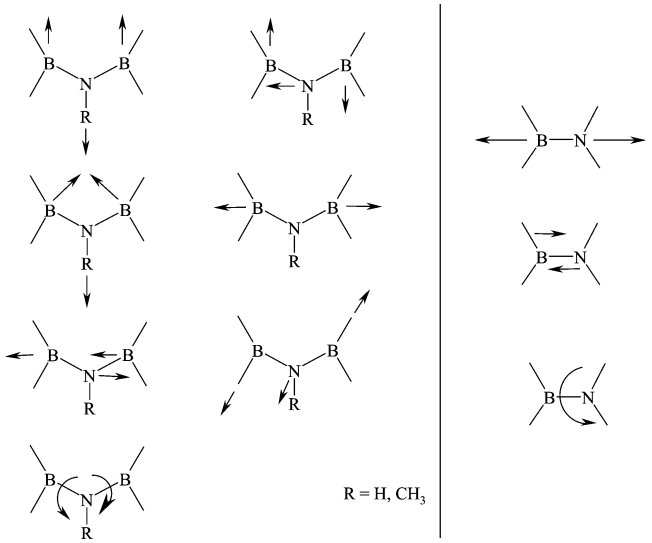

Figure 7. Motion capabilities of the cross-linked sites, i.e., $-N(CH_3)-$ bridges and B−N bonds, which compose the poly[*B*-(methylamino)-borazines] **2**−**6**.

it is reasonable to propose that, at a given degree of cross-linking, adjacent borazine units joined by B−N bonds, i.e., NB_3 sites, restrict molecular motion which naturally stiffens the polymer network, whereas rings branched by bridging units such as $-N(CH_3)-$ bridges provide conformational rearrangements of the polymer backbone and higher freedom in the molecular motion (Figure 7). These bridges therefore add to the flexibility of the polymer backbone.

Therefore, the decrease of both the $-N(CH_3)-$:NB_3 ratio and the relative amounts of $-N(H)CH_3$ groups with increasing $T_{thermolysis}$ involves an increase in the proportion of constraints for molecular motions and a decrease in the plasticity going from **2** to **6**, thereby causing an increase of T_g with increasing $T_{thermolysis}$.

Above T_g, the softened polymer exhibits an appreciable stability and remains stable up to a limit temperature T_l ($T_l = T_g + \sim 100$ °C), at which a strong exothermic peak due to polymer cross-linking is observed in DSC curves. Therefore, poly[*B*-(methylamino)borazine] can be heated in a wide temperature range without change in physical properties and chemical composition. This is an important requirement for performing a stable melt-spinning procedure.

3.3. Polymer Melt-Spinnability. The availability of poly-[*B*-(methylamino)borazines] with "tunable" T_g offers different levels of melt-spinnability.

In the present paper, the spinnability of the samples was first evaluated in terms of capability of extrusion. Melt-spinning was then conducted with the same throughput, with an increasing take-up velocity until the spinning line failed, determining the limit of spinnability, thereby the maximum drawdown ratio.

Spinning was monitored using a high-resolution CCD camera put inside the glovebox and orientated toward the fiber at the exit of the capillary.

Values of the spinning temperatures ($T_{spinning}$), extrusion velocities ($V_{extrusion}$), take-up velocities ($V_{take-up}$), and drawdown ratios[41] defined as $V_{take-up}/V_{extrusion}$ are compiled in Table 4. Together, these variables control the green fiber diameter at the macroscopic level. It should be emphasized that the homogeneity of the fiber diameters given in Table 4 was notable due to high applied take-up velocity which avoided oscillatory instability.

As indicated in Table 4, extrusion of polymers is achieved in a strict and narrow temperature range ($T_{spinning} \pm 1$ °C). By comparison with data (T_g and T_l) reported in Table 3, it is shown that every one of the solid poly[*B*-(methylamino)borazine] studied here is heated at a sufficient temperature ($T_g < T_{spinning} < T_l$) at which they are capable of elastic and plastic deformation to be extruded and drawn without the occurrence of cross-linking and decomposition. Furthermore, these poly[*B*-(methylamino)borazine] can be remelted once they have been spun (not apparent in Table 4) similarly to thermoplastic polymers.

Table 4 also shows that the melt flow behavior is closely related to T_g. Figure 8 even evidence a linear relationship between T_g and $T_{spinning}$ according to eq 2 based on polymers studied here.

$$T_{spinning} = 1.08T_g + 86.34 \quad (2)$$

Figure 8 points to the fact that $T_{spinning}$ is closely related to the cross-linking degree of polymer and the relative amount and nature of structural units which compose the polymer network. Different responses to melt throughput and fiber drawing are logically observed as a function of the polymer architecture using the high-resolution CCD camera.

The low-T_g polymer **2** flows through the capillary at 138 °C ± 1 and emerges as a molten drop at the exit of the capillary (Figure 9a). Relatively high extrusion velocity has to be applied to obtain the ideal spinning pressure (i.e., 350 N), demonstrating the high meltability of such a polymer.

On the basis of the structural features of **2** (i.e., high relative amount of both bridging units (flexibility) and unreacted $-N(H)-CH_3$ groups (plasticity)), we speculate that the borazine rings in **2** are relatively free to move in cooperative thermal motion to provide conformational rearrangement of the backbone and thus high meltability. In contrast, such structural features seem to be an obstacle for the production of continuous **2**-derived fibers of high quality during the subsequent drawing: (i) capillary instability of the filament line upon drawing (Figure 9b) and (ii) loss of fiber cohesion on the take-up spool are observed. Moreover, the molten polymer cross-links too rapidly to be considered for long-term spinning studies. As a consequence, it is appropriate to suggest that a certain degree of cross-linking in the poly[*B*-(methylamino)borazine] network is required to allow for melt-spinning.

Extensive efforts in the design of polymers combining melt extrusion and drawing of the derived filament were made by increasing the final thermolysis temperature $T_{thermolysis}$ above 150 °C.

Increasing thermolysis temperature to 160 and 175 °C provides better melt-spinnability as evidenced by the absence of melt drop during extrusion of the medium-T_g polymers **3** and **4** (Figure 10) at $P \sim 350$ N. The as-extruded molten filament derived from **3** and **4** falls with gravity and can be subsequently drawn from the melt at 155 (**3**) and 165 °C (**4**) without fiber breaking at high take-up velocity ($\kappa = 111.9$). The melt flow remains stable during spinning operation, thus leading to the reproducible preparation of fibers with optimum quality in terms of their smooth surface appearance and uniformity in their low diameter ($d \sim 17.5$ μm). It should be mentioned that a low uniform diameter for green fibers is required for preparing ceramic fibers with high tensile strength after pyrolysis.[20]

Polymers **3** and **4** therefore display excellent extrusion capabilities without capillary fracture most probably due to an adjusted degree of cross-linking. Besides, the appropriate

Table 4. Experimental Spinning Conditions for Poly[*B*-(methylamino)borazine] 2 to 6

polymer	$T_{spinning}$ [°C] (±1)[a]	$V_{extrusion}$ [m/s][b]	$V_{take-up}$ [m/s][c]	κ[d]	exptl fibers diam [μm] (±1)[e]	calcd fiber diam [μm][f]
2	138	0.050			200	
3	155	0.042	4.7	111.9	17.5	18.9
4	165	0.042	4.7	111.9	17.5	18.9
5	175	0.033	3.1	93.9	20.5	21.0
6	195	0.010[g]				

[a] As measured by the thermocouples inside the chamber furnace. [b] Calculated from the piston velocity via volume displacement at a pressure of about 350 N; maximum measured velocity. [c] Maximum measured velocity. [d] Defined as the drawdown ratio, $\kappa = V_{take-up}/V_{extrusion}$; see ref 41. [e] Average of 50 readings taken with the CCD camera and confirmed with a digital micrometer. [f] $d_{fibers} \sim d_{capillary}[(V_{extrusion}/V_{take-up})]^{1/2}$; see ref 41. [g] At $P = 600$ N.

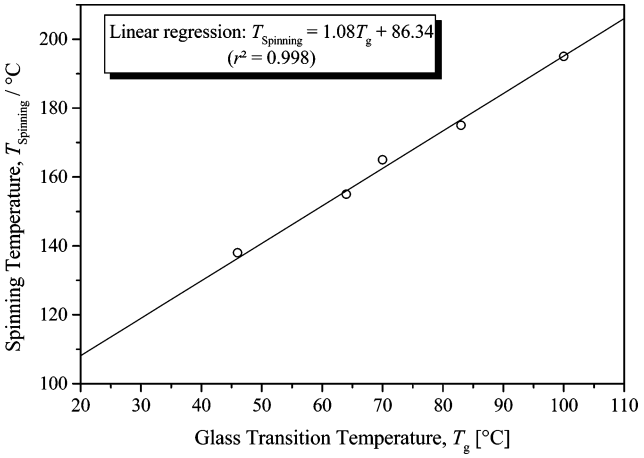

Figure 8. Variation of $T_{spinning}$ a as a function of T_g.

$-N(CH_3)-$ bridges to NB_3 sites ratio in such polymers by controlling $T_{thermolysis}$ provides appropriate stretchability of the as-extruded molten filament, producing green fibers with low diameter. In addition, fiber cohesion was retained after the drawing operation according to a T_g well above RT.

Polymer **5** is readily extrudable at 175 °C ($P \sim 350$ N) with a behavior close to that of polymers **3** and **4** (see Figure 5-SI in Supporting Information). Although the extrusion velocity at $P \sim 350$ N is lower ($V_{extrusion} = 0.033$ m/s) than that used for extrusion of **3** and **4** ($V_{extrusion} = 0.042$ m/s) most probably caused by a lower meltability, the emerging molten filament is drawn at a suitable drawdown ratio ($\kappa = 93.9$), leading to fine-diameter green fibers and defect-free surfaces. At higher drawdown ratios ($\kappa > 93.9$), onset of the polymer jet stretch resonance phenomenon is encountered, and then capillary fracture occurs which can be traced back to the tensile stress undergone by the extruded filament. Using a definite combination of spinning conditions and properties of the polymer being spun through manipulation of the variables reported in Table 4, uniform **5**-based green fibers of ~20.5 μm in diameter are reproducibly obtained. On the basis of such observations, it is therefore reasonable to assume here that the reduced melt-spinnability of green fibers derived from **5** is caused by an increase of both the degree of cross-linking and the relative amount of rigid inter-ring B−N bonds from **4** to **5**. Spinning dynamics were therefore deemed to be conducive to the formation of a stable filament line.

In contrast to polymers **3**−**5**, determination of $T_{spinning}$ for **6** was difficult. For example, extrusion of **6** at 195 °C is barely achieved since the pressure inside the piston chamber quickly increases up to its maximal value, i.e., 600 N, regulating $V_{extrusion}$ to its minimum value, i.e., 0.010 m/s. Such an extrusion behavior clearly shows the lack of meltability of this polymer. It should be mentioned that raising the temperature above 195 °C alters the extrusion, since foam is formed at the exit of the capillary due to thermal decomposition of the polymer.

As the filament emerges, it swells as represented in Figure 11. There was even a tendency for it to fold back on itself rather than fall with gravity, leading to an unstable spinning operation and therefore yielding an irregularly shaped fiber. The as-extruded molten filaments derived therefrom cannot be drawn, and the derived solid green fiber is very stiff and brittle.

Such spinning behavior is related to the high relative amount of NB_3 sites in the polymer network. Referring to unmeltable polyborazylenes, which are composed of both biphenyl and naphthalenic-type structures,[42] it is clear that the natural tendency of NB_3 sites to stiffen the molecule degrades the spinnability of polymer. In contrast to glassy **3**−**5**, **6** represents a crumbly solid that cannot be considered as a candidate for the preparation of fibers.

A final comment on the green fibers derived from poly[*B*-(methylamino)borazines], not apparent in Table 4, concerns the molecular orientation of the polymer chains.

Usually, it is known that on-line drawing may provide substantial molecular orientation.[43] Considering the propensity of poly[*B*-(methylamino)borazines] to cross-link on itself upon heating, it is expected that drawdown ratios reported in Table 4 serve only to maintain filament line stability and control the fiber diameter. However, it is surprising to note that polarized light demonstrates that both on-line fiber extrusion and drawing have also significant effect on molecular orientation in the green fibers derived from poly[*B*-(methylamino)borazines] (Figure 12).

In the case of fibrous materials, as the green fiber is rotated relative to the polarizers, the intensity of the polarization light varies cyclically, from zero (extinction) up to a maximum after 45° and back down to zero after a 90° rotation. Changes in intensity of the polarization light intensities between zero degree (extinction) and 45° (maximum intensity) are poor when as-extruded molten fibers are not drawn during the melt-spinning operation (see Figure 6-SI in Supporting Information), whereas Figure 12 shows that changes are clear when green fibers are drawn, suggesting for the latter a preferred orientation[44] of chains along the fiber axis as an anisotropic material. Such a behavior is not explained at this moment, but it is reasonable to speculate about the possibility to form liquid crystals upon heating and therefore develop a mesophase in our system. The formation of a mesophase in borazine derivatives was already reported,[45] but further studies are needed to demonstrate the formation of such liquid crystals in molten poly[*B*-(methylamino)borazine].

4. Conclusions

The role of the architecture and chemistry of poly[*B*-(methylamino)borazines] on the thermal and spinning behaviors is explored in this study. Using *B*-(methylamino)borazine as molecular precursor, derived poly[*B*-(methylamino)borazines] with different degree of cross-linking are recovered by adjusting the final thermolysis temperature between 150 and 200 °C. These polymers may be represented by a structural network combining cross-linked portions of the type $-N(CH_3)-$ bridges (major) and B−N bonds (minor) which connect borazine units

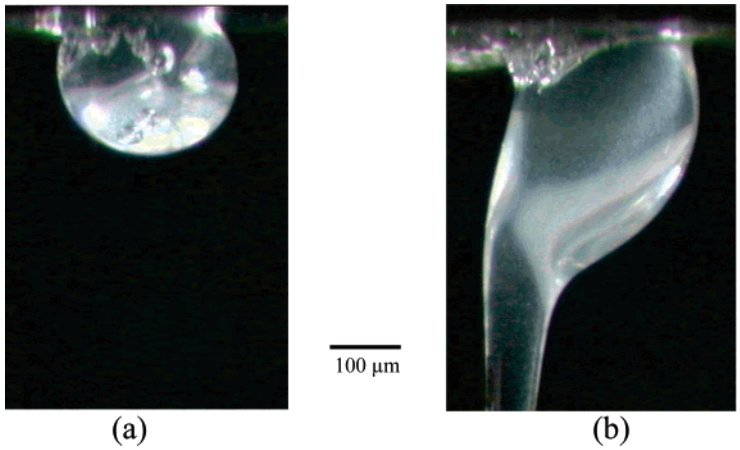

Figure 9. As-spun fiber drawn from the molten poly[*B*-(methylamino)borazine] **2** using a pressure of about 350 N and an extrusion velocity of 0.050 m/s.

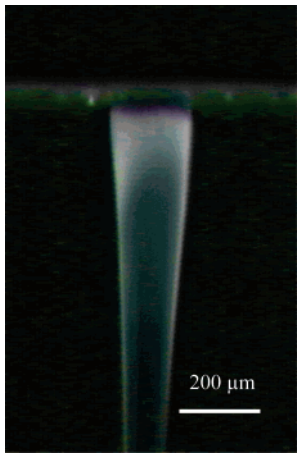

Figure 10. As-spun fiber drawn from molten poly[*B*-(methylamino)-borazine] **3** and **4** using a pressure of about 350 N and an extrusion velocity of 0.042 m/s.

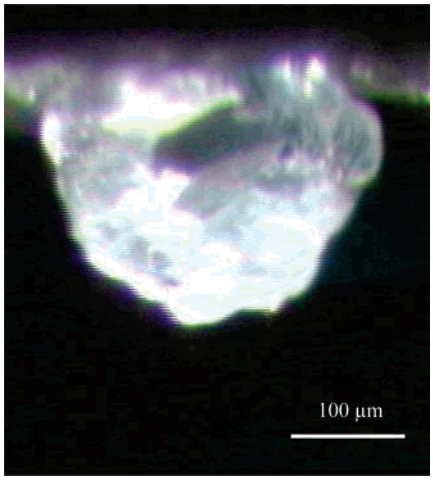

Figure 11. As-spun fiber drawn from the molten poly[*B*-(methylamino)borazine] **6** using a pressure of 600 N.

together. Polymer chains are capped by $-N(H)CH_3$ groups whose relative amount decreases with increasing thermolysis temperature ($T_{thermolysis}$). Whereas $-N(CH_3)-$ bridges are preferentially formed in the low-temperature regime of the thermolysis process ($T_{thermolysis} \leq 160$ °C), formation of interring B−N bonds occurs in the high-temperature regime ($T_{thermolysis} > 160$ °C). Such behaviors do not involve significant changes in the chemical composition of polymers, but our results show that these architecture changes cause strong variation in the thermal behavior and melt-spinnability of such polymers. Ideal melt-spinnable poly[*B*-(methylamino)-borazines] are obtained between 160 and 185 °C. Such typical melt-spinnable polymers display a chemical formula of $[B_{3.0}N_{4.4\pm0.1}C_{2.0\pm0.1}H_{9.3\pm0.2}]_n$ ($n \sim 7.5$) and glass transition temperatures in the range 64−83 °C. These features provide adjusted flexibility determined by the $-N(CH_3)-$:NB_3 ratio and sufficient plasticity given by the relative amount of $-N(H)-CH_3$ groups to prepare fine-diameter green fibers at 165 ± 10 °C in a stable melt-spinning operation. In the following paper, the shear rheology of polymer melts is investigated to understand how the structural features of poly[*B*-(methylamino)borazines] can affect the rheological behavior. This rheological investigation provides a detailed picture of the architecture−rheology−spinnability relationship.

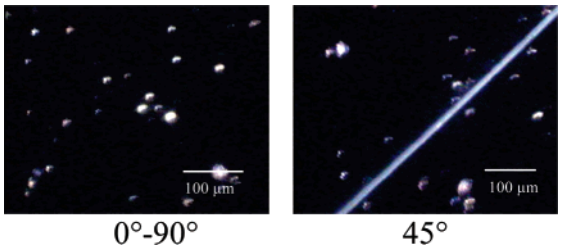

Figure 12. Green fiber derived from the molten poly[*B*-(methylamino)-borazine] **4** with drawing.

Acknowledgment. The authors gratefully acknowledge supporting co-workers at the LMI in Lyon, Dr. Jean-Marie Létoffé (DSC) for his contribution to thermal analyses, and Dr. Fernand Chassagneux for the density measurements. In addition, they thank Hicham Moutaabbid for the CCD pictures, René Fulchiron from the LMPB (UMR CNRS 5627) for his investigation in polarized light, and Gerhard Kaiser at the PML (Department of Prof F. Aldinger) in Max-Planck Institute of Stuttgart for elemental analysis. We thank the European Community who supported this work through the Marie Curie Research Training Network PolyCerNet (Contract MRTN-CT-2005-019601).

Supporting Information Available: Figures 1-SI to 6-SI and Schemes 1-SI and 2-SI. This material is available free of charge via the Internet at http://pubs.acs.org.

References and Notes

(1) Peuckert, M.; Vaahs, T.; Brück, M. *Adv. Mater.* **1990**, *2*, 398.
(2) Bill, J.; Aldinger, F. *Adv. Mater.* **1995**, *7*, 775.
(3) Laine, R. M.; Sellinger, A. *Si-Containing Ceramic Precursors in the Chemistry of Organic Silicon Compounds*; Patai, S., Rappoport, Z., Eds.; John Wiley & Sons: New York, 1998; Vol. 2, Chapter 39, p 2245.
(4) Chantrell, P. G.; Popper, E. P. In *Special Ceramics-4*; Popper, E. P., Ed.; Academic Press: New York, 1964; p 87.
(5) Yajima, S.; Shishido, T.; Kayano, H. *Nature (London)* **1978**, *273*, 525.
(6) Winter, G.; Verbeek, W.; Mansmann, M. U.S. Patent 3,892,583, 1975.
(7) Zhang, Z.-F.; Scotto, C. S.; Laine, R. M. *J. Mater. Chem.* **1998**, *8*, 2715.
(8) Motz, G.; Hacker, J.; Ziegler, G.; Clauss, B.; Schawaller, D. Low-Cost-Ceramic SiCN Fibers By an Optimized Polycarbosilazane and Continuous Processing. In *Inorganic Structural Fiber Composites*; Vincenzini, P., Badini, C., Eds.; 2003; p 47.
(9) Bernard, S.; Weinmann, M.; Gerstel, P.; Miele, P.; Aldinger, F. *J. Mater. Chem.* **2005**, *5*, 289.
(10) Wynne, K. J.; Rice, R. W. *Annu. Rev. Mater. Sci.* **1984**, *14*, 297.
(11) Tanigushi, L.; Harada, K.; Maeda, T. *Chem. Abstr.* **1976**, *85*, 96582v.
(12) Wideman, T.; Sneddon, L. G. *Chem. Mater.* **1996**, *8*, 3.
(13) Paine, R. T.; Narula, C. K. *Chem. Rev.* **1990**, *90*, 73.
(14) Allcock, H. R.; Welker, M. F.; Parvez, M. *Chem. Mater.* **1992**, *4*, 296.
(15) Paine, R. T.; Sneddon, L. G. *CHEMTECH* **1994**, *24*, 29.
(16) Toury, B.; Miele, P.; Cornu, D.; Vincent, H.; Bouix, J. *Adv. Funct. Mater.* **2002**, *12*, 228.
(17) Bernard, S.; Cornu, D.; Miele, P.; Vincent, H.; Bouix, J. *J. Organomet. Chem.* **2002**, *657*, 91.
(18) Toury, B.; Bernard, S.; Cornu, D.; Chassagneux, F.; Letoffe, J.-M.; Miele, P. *J. Mater. Chem.* **2003**, *13*, 274.
(19) Lindquist, D. A.; Janik, J. F.; Datye, A. K.; Paine, R. T. *Chem. Mater.* **1992**, *4*, 17.
(20) Bernard, S.; Chassagneux, F.; Berthet, M. P.; Vincent, H.; Bouix, J. *J. Eur. Ceram. Soc.* **2002**, *22*, 2047.
(21) Bernard, S.; Fiaty, K.; Cornu, D.; Miele, P.; Laurent, P. *J. Phys. Chem. B* **2006**, *110*, 9048.
(22) Bernard, S.; Chassagneux, F.; Berthet, M.-P.; Cornu, D.; Miele, P. *J. Am. Ceram. Soc.* **2005**, *88*, 1607.
(23) Richter, R.; Roewer, G.; Böhme, U.; Busch, K.; Babonneau, F.; Martin, H. P.; Müller, E. *Appl. Organomet. Chem.* **1997**, *11*, 71.
(24) Wang, Y.; Song, Y.; Feng, C.; Zou, Z.; Zhao, Y.; Long, J. *Key Eng. Mater.* **1999**, *33*, *164*−165.
(25) Idesaki, A.; Narisawa, M.; Okamura, K.; Sugimoto, M.; Tanaka, S.; Morita, Y.; Seguchi, T.; Itoh, M. *J. Mater. Sci.* **2001**, *36*, 5565.
(26) Legrow, G. E.; Lim, T. F.; Lipowitz, J.; Reaoch, R. S. *Am. Ceram. Soc. Bull.* **1987**, *66*, 363.
(27) Lücke, J.; Hacker, J.; Sutter, D.; Ziegler, G. *Appl. Organomet. Chem.* **1997**, *11*, 181.
(28) Duperrier, S.; Gervais, C.; Bernard, S.; Cornu, D.; Babonneau, F.; Miele, P. *J. Mater. Chem.* **2006**, *16*, 3126.
(29) Gervais, C.; Maquet, J.; Babonneau, F.; Duriez, C.; Framery, E.; Vaultier, M.; Florian, P.; Massiot, D. *Chem. Mater.* **2001**, *13*, 1700.
(30) Gervais, C.; Babonneau, F.; Maquet, J.; Bonhomme, C.; Massiot, D.; Framery, E.; Vaultier, M. *Magn. Reson. Chem.* **1998**, *36*, 407.
(31) Massiot, D.; Fayon, F.; Capron, M.; King, I.; Le Calvé, S.; Alonso, B.; Durand, J.-O.; Bujoli, B.; Gan, Z.; Hoatson, G. *Magn. Reson. Chem.* **2002**, *40*, 70.
(32) Toury, B.; Gervais, C.; Dibandjo, P.; Cornu, D.; Miele, P.; Babonneau, F. *App. Organomet. Chem.* **2004**, *18*, 227.
(33) Lappert, M. F. *Proc. Chem. Soc.*, **1959**, 59. Lappert, M. F.; Majunder, M. K. *Proc. Chem. Soc.* **1962**, 425. Aubrey, D. W.; Lappert, M. F. *J. Chem. Soc.* **1959**, 2927.
(34) Kimura, Y.; Kubo, Y.; Hayashi, N. *Compos. Sci. Technol.* **1994**, *51*, 173.
(35) Paciorek, K. J. L.; Kratzer, R. H.; Harris, D. H.; Smythe, M. E. *Polym. Prepr.* **1984**, *25*, 15.
(36) Gerrard, W.; Hudson, H. R.; Mooney, E. F. *J. Chem. Soc.* **1962**, 113.
(37) Toeniskoetter, R. H.; Hall, F. R. *J. Am. Chem. Soc.* **1963**, *84*, 4619.
(38) Kimura, Y.; Kubo, Y.; Hayashi, N. *J. Inorg. Organomet. Polym.* **1992**, *2*, 231.
(39) Fontanille, M.; Gnanou, Y. In *Chimie et Physico-chimie des polymères*; Dunod, Ed.; Paris, 2002.
(40) Mathot, V. B. F. In *Calorimetry and Thermal Analysis of Polymers*; Hanser, Ed.; 1994.
(41) Edie, D. D.; Dunham, M. G. *Carbon* **1989**, *27*, 647.
(42) Fazen, P. J.; Beck, J. S.; Lynch, A. T.; Remsen, E. E.; Sneddon, L. G. *Chem. Mater.* **1990**, *2*, 96.
(43) Murase, Y.; Nagai, A. In *Advanced Fiber Spinning Technology*; Nakajima, T., Ed.; Woodhead Publishing: Cambridge, 1994.
(44) Garvey, D. W.; Zimmerman, K.; Young, P.; Tostenrude, J.; Townsend, J. S.; Zhou, Z.; Lobel, M.; Dayton, M.; Wittorf, R.; Kuzyk, M. G.; Sounick, J.; Dirk, C. W. *J. Opt. Soc. Am. B* **1996**, *13*, 2017.
(45) Kim, D.-P.; Economy, J. *Chem. Mater.* **1994**, *6*, 395.

MA0623035